



# Rh-Catalyzed Cycloaddition of C<sub>60</sub> with Enynes: Unveiling the Mechanistic Pathway

Cristina Castanyer,<sup>a</sup> Albert Artigas,<sup>a,\*</sup> Nil Insa-Carreras,<sup>a</sup> Miquel Solà,<sup>a</sup>  
Anna Pla-Quintana,<sup>a,\*</sup> and Anna Roglans<sup>a,\*</sup>

<sup>a</sup> Institut de Química Computacional i Catàlisi (IQCC) and Departament de Química, Universitat de Girona (UdG), Facultat de Ciències, C/Maria Aurèlia Capmany, 69, 17003-Girona, Catalunya, Spain  
E-mail: anna.roglans@udg.edu; anna.plaq@udg.edu; albert.artigas@udg.edu

Manuscript received: October 18, 2023; Revised manuscript received: November 16, 2023;  
Version of record online: January 4, 2024

 Supporting information for this article is available on the WWW under <https://doi.org/10.1002/adsc.202301189>

 © 2024 The Authors. Advanced Synthesis & Catalysis published by Wiley-VCH GmbH. This is an open access article under the terms of the Creative Commons Attribution Non-Commercial NoDerivs License, which permits use and distribution in any medium, provided the original work is properly cited, the use is non-commercial and no modifications or adaptations are made.

**Abstract:** In this study we present a method for functionalizing C<sub>60</sub> through a Rh-catalyzed cyclization reaction with 1,6-enynes, resulting in the formation of a fused bicyclic structure. Additionally, fullerene derivatives are further functionalized through regioselective photooxygenation reactions. Our DFT calculations reveal two distinct reaction pathways: one involving rhodium-catalyzed cycloisomerization of the enyne followed by Diels-Alder with C<sub>60</sub>, and the other featuring a rhodium-catalyzed [2+2+2] cycloaddition of enyne and C<sub>60</sub> followed by isomerization. Surprisingly, both pathways exhibit nearly identical energy barriers. However, experimental tests indicate that the predominant pathway varies depending on the substitution motifs of the substrates.

**Keywords:** Cycloaddition; 1,6-enynes; Fullerene; Rhodium; Density Functional Calculations

## Introduction

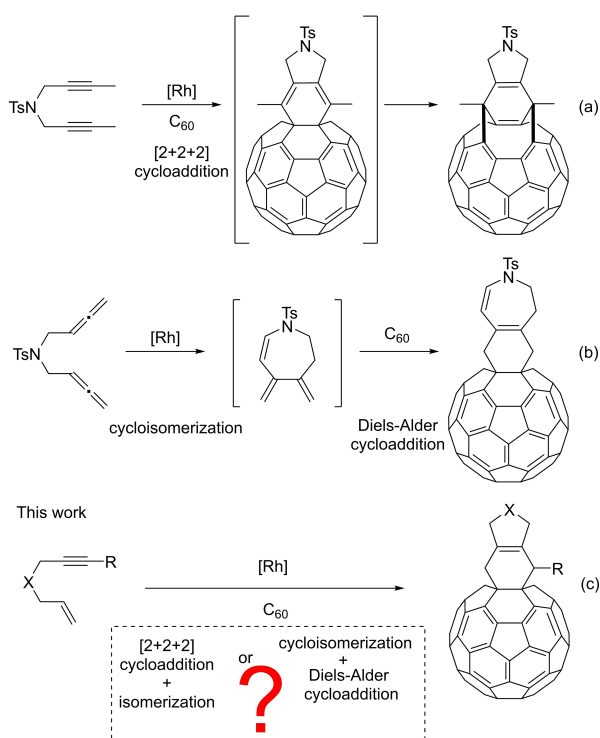
Exohedrally modified fullerenes have attracted significant attention due to their remarkable applications in various fields such as biomedicine,<sup>[1]</sup> materials science,<sup>[2]</sup> and next-generation photovoltaics.<sup>[3]</sup> This has led to the exciting goal of achieving tailored and selective decorations on this molecular architecture. A crucial aspect for this purpose is the higher reactivity of the double bonds present in the junctions between two six-membered rings of fullerene cages, commonly referred to as [6,6] bonds. These bonds, which are shorter and exhibit double bond character actively participate in numerous chemical reactions, with cycloaddition reactions playing a pivotal role.<sup>[4]</sup>

Among cycloadditions, those most widely used to functionalize fullerenes are the Diels-Alder, the 1,3-dipolar cycloadditions, and the Bingel-Hirsch cyclopropanations.<sup>[5]</sup> While the conditions for the monofunctionalization reaction are generally possible,

these reactions are prone to polyfunctionalization leading to an intractable mixture of regioisomers.<sup>[6]</sup>

Although much less developed, transition metal-catalyzed cycloaddition reactions of C<sub>60</sub> with unsaturated scaffolds represent a fundamental tool for the construction of complex cyclic compounds fused to fullerenes and generally do not suffer from polyadditions.<sup>[7]</sup>

Rhodium is known to catalyze a vast range of cycloaddition and cycloisomerization reactions of unsaturated substrates. In an ongoing project from our group, we described two different reactivity patterns in the functionalization of fullerenes. On the one hand, the [2+2+2] cycloaddition involving C<sub>60</sub> as one of the reactive unsaturations (Scheme 1a),<sup>[8]</sup> and on the other hand, a cycloisomerization of a bisallene substrate, generating *in situ* a reactive diene that engages in a Diels-Alder cycloaddition with a [6,6] bond of C<sub>60</sub> (Scheme 1b).<sup>[9]</sup> Whereas in the latter polyadditions were clearly detected, the rhodium-catalyzed [2+2+2] cycloaddition was never observed to take place on a



**Scheme 1.** Rh-catalyzed cycloaddition reactions of C<sub>60</sub> with (a) 1,6-diynes,<sup>[8]</sup> (b) 1,5-bisallenyls,<sup>[9]</sup> and (c) 1,6-enynes.

monofunctionalized fullerene. Motivated by these findings and intrigued by the diverse behavior exhibited by different unsaturated substrates, our interest shifted to 1,*n*-enynes. The key question at hand was whether these substrates would engage in a [2+2+2] cycloaddition reaction with C<sub>60</sub> or trigger a cascade process based on a cycloisomerization, followed by a Diels-Alder reaction with the pristine fullerene (Scheme 1c).

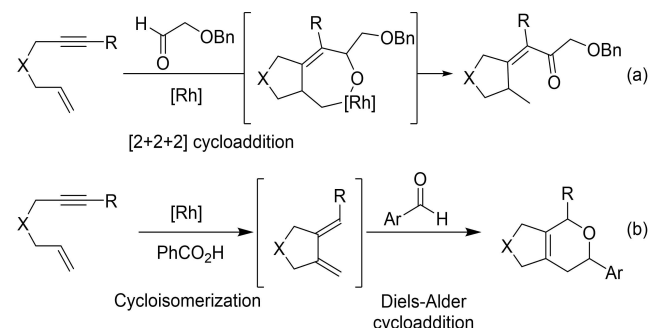
1,*n*-Enynes have emerged as an extremely attractive starting material for cycloisomerization and cycloaddition reactions. Since the pioneering study by Trost,<sup>[10]</sup> enynes -and particularly 1,6-enynes- have attracted considerable attention as valuable building blocks for accessing a myriad of cyclic compounds in an atom-economic processes under mild reaction conditions. Enynes exhibit versatility by undergoing various cycloisomerization processes under transition metal catalysis<sup>[11]</sup> or by participating in cycloadditions with a third unsaturation, the relevant cases of which are the Pauson-Khand reaction<sup>[12]</sup> and the [2+2+2] cycloaddition reaction.<sup>[13]</sup> In the former scenario, cycloisomerization of enynes can afford cyclized 1,3-dienes, which can be used as dienes in Diels-Alder reactions in cascade processes.<sup>[14]</sup> Fuller-1,6-enynes can participate in a thermal [2+2] intramolecular cyclization to generate three fused rings on the same hexagonal ring of the fullerene surface containing a cyclobutene moiety.<sup>[15]</sup>

An example of the two different types of reactivity can be seen in the works by Tanaka et al.<sup>[16,17]</sup> shown in Scheme 2. The reaction of enynes with chelating alkoxyacetaldehydes under rhodium catalysis and in the presence of (*R*)-BINAP ligand took place via an enantioselective [2+2+2] cycloaddition reaction (Scheme 2a).<sup>[16]</sup> Conversely, when the reaction was carried out with arylaldehydes and in the presence of a Brønsted acid, the former favoured the cycloisomerization of the enyne to give an exocyclic 1,3-diene, which subsequently reacts with the aldehyde to give hetero-Diels-Alder reaction in a cascade process (Scheme 2b).<sup>[17]</sup> In these cases, both the nature of the starting aldehyde and the reaction conditions direct the course of the cycloaddition giving different products.

Considering the potential that enynes can have in cycloaddition reactions and visualizing a method to functionalize fullerenes, here we report our findings with regard to the reaction of 1,6-enynes with C<sub>60</sub> under rhodium catalysis (Scheme 1c). By investigating the mechanistic pathway by DFT calculations, we aim to gain valuable insights into these types of reactions.

## Results and Discussion

The study was initiated by testing the reaction conditions for the cycloaddition between fullerene C<sub>60</sub> and *N*-tosyl-tethered enyne **1a** (see Table 1 and Table S1 in the Supporting Information). In our initial attempts, an equimolar mixture of a cationic rhodium complex [Rh(cod)<sub>2</sub>]BF<sub>4</sub> (cod=cyclooctadiene) and (*R*)-Tol-BINAP, pre-treated under hydrogenation conditions, was used as a catalyst. Upon heating the reaction mixture for 30 min in refluxing *o*-dichlorobenzene (*o*-DCB) and using an excess of enyne **1a** (3 equiv. with respect to C<sub>60</sub>), product **2a** was obtained in a 56% yield (entry 1, Table 1). The equivalents of the enyne were then reduced to 2 (entry 2, Table 1), the solvent was changed to toluene (entry 3, Table 1) and the temperature was lowered to 70 °C (entry 4, Table 1) but none of these three modifications improved yields of **2a**. The temperature of 90 °C appears to be crucial



**Scheme 2.** Examples of the versatility of enynes in cycloaddition reactions.<sup>[16,17]</sup>

**Table 1.** Optimization of the rhodium(I)-catalyzed cycloaddition of enyne **1a** with fullerene  $C_{60}$ .<sup>[a]</sup>

Entry	Ligand	Solvent/T (°C)	t (min)	Yield (%)
1	( <i>R</i> )-Tol-BINAP	<i>o</i> -DCB/90	30	56
2 <sup>[b]</sup>	( <i>R</i> )-Tol-BINAP	<i>o</i> -DCB/90	30	42
3	( <i>R</i> )-Tol-BINAP	Toluene/90	30	37
4	( <i>R</i> )-Tol-BINAP	<i>o</i> -DCB/70	30	0
5	BIPHEP	<i>o</i> -DCB/90	30	50
6	( <i>R</i> )-DTBM-Segphos	<i>o</i> -DCB/90	30	31
7	Xantphos	<i>o</i> -DCB/90	60	26
8	( <i>R</i> )-Segphos	<i>o</i> -DCB/90	30	34
9	( <i>rac</i> )-BINAP	<i>o</i> -DCB/90	30	32
10	XPhos	<i>o</i> -DCB/90	90	0

<sup>[a]</sup> Reaction conditions: 0.07 mmol of  $C_{60}$ , 3 equiv. of **1a**, 10 mol% of Rh catalyst in *o*-DCB (1.4 mM) at the indicated temperature and time. The 10 mol% mixture of  $[Rh(cod)_2]BF_4$  and phosphine ligand was treated with hydrogen in dichloromethane ( $CH_2Cl_2$ ) solution for catalyst activation prior to substrate addition.

<sup>[b]</sup> 2 equiv. of **1a** were used.

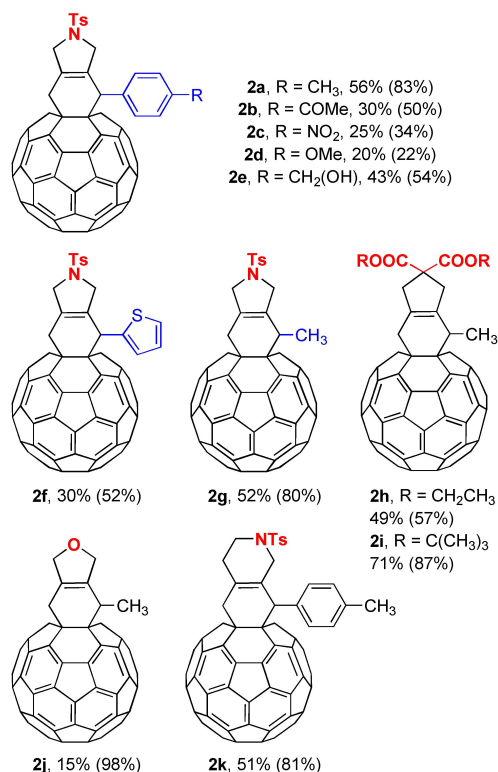
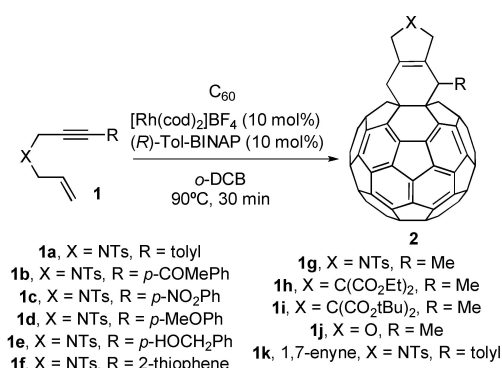
for the successful completion of the reaction (compare entries 1 and 4 in Table 1). Further optimization of the reaction conditions was attempted by varying the ligand. The use of biaryl biphosphines other than (*R*)-Tol-BINAP (entries 5–9, Table 1) or monophosphine XPhos (entry 10, Table 1) proved to be less effective. Finally, two blank experiments were conducted indicating that the presence of Rh and ligand was required for the success of the process (see Table S1 in the Supporting Information).

The structure of **2a** was unambiguously characterized using HRMS, NMR ( $^1H$ ,  $^{13}C$ , COSY, HSQC, and HMBC), and UV-Vis spectra. The molecular formula of this compound was determined to be  $C_{80}H_{21}NO_2S$  by ESI-HRMS ( $[M+Na]^+$ ,  $m/z = 1082.1203$ ), indicating the formation of a monoadduct. The  $^1H$  NMR spectrum of **2a** exhibited a singlet signal at 5.26 ppm confirming by HSQC that this is the only  $C_{sp^3}H$  group (H4 in scheme of Table 1) (C at 54.4 ppm) in the structure. This is key in making the deduction that the double bond is in the ring junction between the two rings of the addend. In addition, for the protons in the  $\alpha$ -position of the nitrogen atom, two sets of diastereotopic protons are observed. For position 2, two broad doublet signals at 4.39 and 4.94 ppm ( $^2J = 14.4$  Hz) are assigned and a multiplet signal at around 4.70 ppm is assigned to protons at position 3. Finally, a multiplet at

4.10 ppm corresponding to the two methylene protons in position 1 appeared in the spectrum (C atom at 39.4 ppm). These two protons, together with the proton at position 4, showed correlation with carbon atoms of the fullerene cage by HMBC.

The UV-Vis absorption spectrum showed an absorption band at 432 nm, which is in accordance with the characteristic pattern expected for a cyclohexene-fused  $C_{60}$  monoadduct.<sup>[9]</sup> Taken together all this data allowed us to unambiguously identify the product formed as **2a**.

With an optimized set of conditions at hand (entry 1, Table 1), the scope of the reaction was then examined (Scheme 3). With *N*-tosyl tethered-enynes,

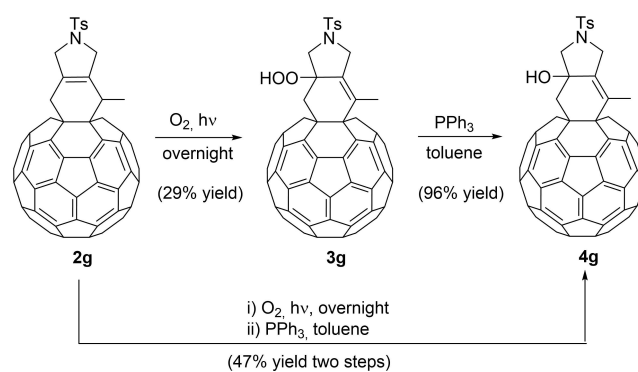


**Scheme 3.** Scope of the cycloaddition of enynes **1a–1k** with  $C_{60}$ . The values in parentheses are the yields based on the amount of  $C_{60}$  consumed.

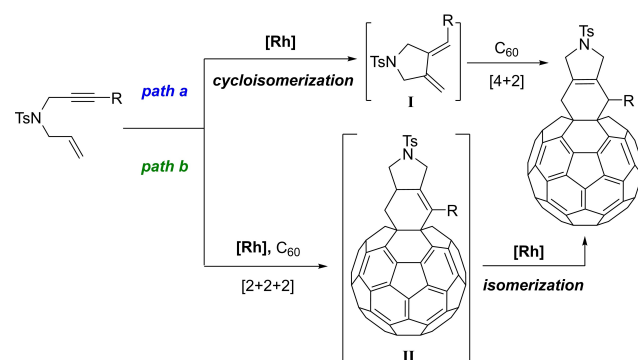
several phenyl-substituted groups (with electron-donating and electron-withdrawing groups) at the terminus of the alkyne were tolerated in the process and fullerene derivatives **2a–2e** were obtained with moderate to good yields. An enyne with a heteroaromatic ring at the alkyne terminus, such as thiophene, successfully underwent a reaction, resulting in the formation of derivative **2f** with a 30% yield. With regard to the substituent in the alkyne, not only aromatic scaffolds but also a methyl-substituted alkyne reacted with fullerene, to give compound **2g** with a 52% of yield. We then explored whether 1,6-enynes with a tether other than nitrogen could also yield favorable reactions. Diethyl and *tert*-butylmalonate were tested as tethering units in the enyne with a methyl substituent in the alkyne, providing a 49% and 71% yield of the fullerene derivatives **2h** and **2i**, respectively. In addition, an oxygen linkage could also be used in the cycloaddition although final product **2j** was obtained in a low yield. Finally, a 1,7-enyne was also tested to obtain a [6,6]-ring fusion in the fullerene derivative. In this case, the reaction was successful, resulting in the formation of compound **2k** with a 51% yield.

Due to the photophysical properties of  $C_{60}$ , this compound and its derivatives serve as efficient photosensitizers capable of generating singlet oxygen under irradiation. Singlet molecular oxygen ( $^1O_2$ ) readily reacts with organic compounds. An example of this is the reaction between alkenes and oxygen, which results in the formation of allylic alcohols by regioselective extraction of hydrogen from an allylic position on the substrate.<sup>[18]</sup> Fullerenes functionalized with a cyclohexene ring can undergo photooxidation through an ene reaction with singlet oxygen to generate allylic hydroperoxides that can subsequently be reduced to their respective allylic alcohols.<sup>[19]</sup> With this idea in mind, fullerene derivative **2g** was irradiated with a conventional lamp in the presence of air to afford hydroperoxide **3g** with a 29% yield in a regioselective manner. Further reduction with triphenylphosphine afforded the allylic alcohol derivative **4g** with a 96% yield. The two reactions could be done in one step, without isolating the hydroperoxide, obtaining **4g** with an improved overall yield of 47% (Scheme 4).

Once we established a method to functionalize  $C_{60}$  with enynes under rhodium catalysis, we were intrigued by the mechanism that governs the whole process. We considered two plausible reaction pathways leading to the formation of cycloadducts **2**. These pathways include: (i) A [4+2] Diels-Alder reaction of  $C_{60}$  with cyclopentadiene intermediate **I**, which would be generated through a Rh(I)-catalyzed cycloisomerization (path a in Scheme 5); and (ii) a Rh-catalyzed [2+2+2] cycloaddition reaction to form intermediate **II**, followed by a Rh-catalyzed isomerization of the double bond (path b in Scheme 5). To this aim, both



**Scheme 4.** Photooxygenation of fullerene derivative **2g** and further reduction to derivative **4g**.



**Scheme 5.** The two mechanistic hypotheses considered in our DFT study.

mechanisms were studied and compared by density functional theory (DFT) calculations at the B3LYP-D3/cc-pVTZ(SMD= $\rho$ -DCB)//B3LYP-D3/cc-pVDZ level of theory ( $T=363.15$  K, see computational details) (Figures 1 and 2). To minimize computational expenses, we employed methyl-substituted enyne **1g** ( $R=Me$ ) as a model substrate.

Both reaction pathways begin with the coordination of the Rh complex to enyne **1g**, forming intermediate **A1** ( $\Delta G = -2.2$  kcal·mol<sup>-1</sup>). Subsequently, **A1** experiences an oxidative coupling to give rhodacyclopentene intermediate **A2**. This step exhibits a minor exergonicity of 1.4 kcal·mol<sup>-1</sup> and occurs *via* **TS A1A2**, with a barrier of 23.9 kcal·mol<sup>-1</sup> in its most stable conformation. We have also considered alternative conformations of **A1**, **A2**, and **TS A1A2**, as detailed in Figure S1 of the Supporting Information. The ones depicted in Figures 1 and 2 represent the lowest energy path. From **A2**, the two reaction paths diverge. In path a (Figure 1), **A2** is transformed into Rh-H intermediate **A3** through a  $\beta$ -hydride elimination mechanism. This step has a high cost of 30.1 kcal·mol<sup>-1</sup> and is endergonic by 6.2 kcal/mol. Then, intermediate **A3** readily undergoes reductive elimination (**TS A3A4**), resulting in **A4**, which ultimately releases intermediate **I** and

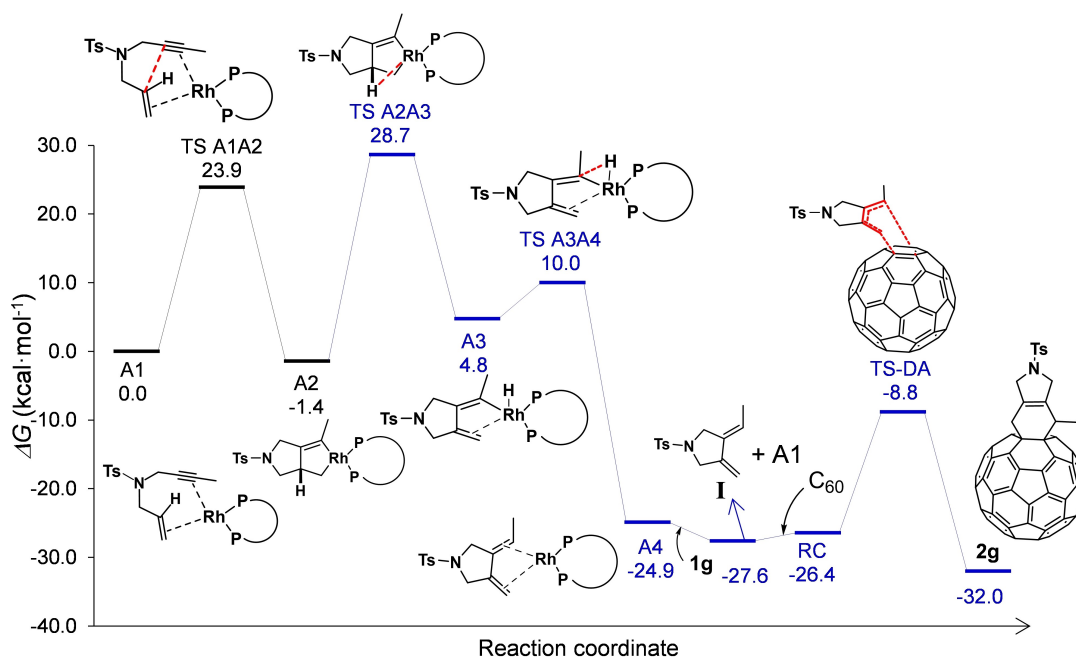


**Figure 1.** B3LYP-D3/cc-pVTZ(SMD = *o*-DCB)//B3LYP-D3/cc-pVDZ Gibbs energy profile computed at 363.15 K of the Rh-catalyzed reaction between  $C_{60}$  and enyne **1g** (path a).

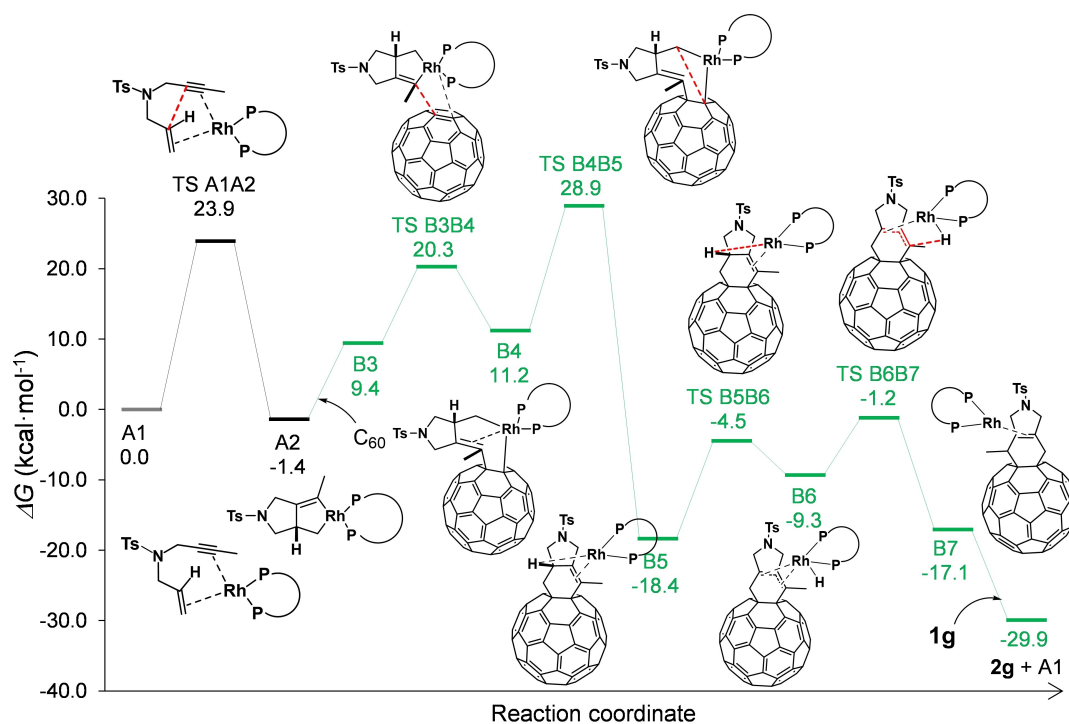


**Figure 2.** B3LYP-D3/cc-pVTZ(SMD = *o*-DCB)//B3LYP-D3/cc-pVDZ Gibbs energy profile computed at 363.15 K of the Rh-catalyzed reaction between  $C_{60}$  and enyne **1g** (path b).

regenerates **A1** by the entrance of another molecule of substrate (**1g**) into the catalytic cycle. These two consecutive steps have a low barrier of  $5.2 \text{ kcal} \cdot \text{mol}^{-1}$  and are exergonic by  $32.4 \text{ kcal} \cdot \text{mol}^{-1}$ . Intermediate **I** is

a reactive diene that can react with fullerene  $C_{60}$  in a Diels-Alder cycloaddition to deliver reaction product **2g**. The overall process exhibits a substantial exergonicity of  $32.0 \text{ kcal} \cdot \text{mol}^{-1}$  and has a Gibbs energetic

span ( $\delta G$ )<sup>[20]</sup> between the turnover frequency (TOF) determining intermediate (TDI, **A2**) and the TOF determining transition state (TDTS, **TS A2A3**) of 30.1 kcal·mol<sup>-1</sup>.

On the other hand, in path b (Figure 2), intermediate **A2** can coordinate a [6,6] bond of a C<sub>60</sub> molecule to provide intermediate **B3** in an endergonic process that has a cost of 10.8 kcal·mol<sup>-1</sup>. Subsequently, insertion of this double C-C bond *via* Schore's mechanism<sup>[21]</sup> yields rhodacycloheptene intermediate **B4**, which is then converted into **B5** *via* reductive elimination. As a whole, the mechanistic steps that transform **A2** into cyclohexene intermediate **B5** are exergonic by 17.0 kcal·mol<sup>-1</sup> and have a barrier of 30.3 kcal·mol<sup>-1</sup>. Importantly, in **B5**, the rhodium centre is located in close proximity (1.97 Å) to the hydrogen atom of the C<sub>sp3</sub> at the junction between the 5- and 6- membered rings of the addend. This particular feature facilitates a  $\beta$ -hydride elimination step that occurs through a relatively accessible barrier (**TS B5B6**) of 13.9 kcal·mol<sup>-1</sup> (vs. 30.1 in path a).

The resulting Rh-H intermediate **B6** is finally converted into the final product *via* reductive elimination (**TS B6B7**) and catalyst release by substitution with another unit of **1g**, restarting the catalytic cycle. The whole process was found exergonic by 29.9 kcal·mol<sup>-1</sup> and has a  $\delta G$  between the TDI (**A2**) and the TDTS (**TS B4B5**) of 30.3 kcal·mol<sup>-1</sup>.

As discussed in the preceding paragraphs, the two mechanisms that have been studied have almost identical barriers. Therefore, from the results obtained, we deduced that both paths a and b may be involved in the transformation of C<sub>60</sub> and enynes **1** into cycloadducts **2**. To gain a better understanding of the process, we decided to experimentally investigate the reaction mechanism further. We reasoned that if path a was the dominant route, an elevated concentration of enyne **1g** in the reaction medium should promote polyaddition of intermediate **I** on C<sub>60</sub>. The occurrence of polyadducts in DA reactions involving fullerenes has been well-documented.<sup>[6]</sup> Most notably, the Rh-catalyzed reaction of C<sub>60</sub> with bisallenes, which has been established as proceeding through the cycloisomerization/[4+2] pathway,<sup>[9,22]</sup> results in the formation of *bis* and *tris* adducts when an excess of bisallene is present in the reaction mixture. Similarly, when reacting C<sub>60</sub> in the presence of 6 equiv. of **1g** (vs. 3 equiv. in the optimized reaction conditions), we observed the progressive disappearance of cycloadduct **2g**, together with the appearance of more retained spots on the TLC plate, which was attributed to polyaddition products by MALDI-MS experiments. Moreover, it was possible to isolate intermediate **I** (27% yield) using these reaction conditions (See Supporting Information). Isolation of intermediate **I** shows the pivotal role of this intermediate in the global process and, in light of these results, it may be

concluded that path a operates for the formation of **2g**. Conversely, when performing the same experiment in the presence of excess **1a** (6 equiv.), the spot attributed to the monoadduct remained unaltered after 30 min of reaction.<sup>[23]</sup> Additionally, no traces of *bis* or *tris* adducts were detected by MALDI-MS experiments in any of the fractions eluted after **2a** by column chromatography. Similar behaviour was observed in the case of the [2+2+2] cycloaddition of diynes and C<sub>60</sub>,<sup>[8a]</sup> suggesting that path b is the predominant pathway for **2a** under the tested conditions. Thus, the fact that subtle structural difference led to significantly distinct outcomes again reinforces the equal feasibility of the two mechanisms and they can both come into play during the reaction depending on the specific conditions and reactants used.

## Conclusion

In conclusion, we have developed a method to synthesize a series of fullerene adducts bearing 5,6-membered polyheterocyclic addends. A combination of DFT calculations and experimental evidence allowed us to shed light on the mechanism of the reaction, which can take place through two different pathways depending on the substrates used. In addition, the photooxygenation reaction of the synthesized fullerene derivatives can concomitantly affect the chemical modification of the cyclohexene framework to give regioselectively interesting oxygenated systems.

## Experimental Section

### General Procedure for the Synthesis of Derivatives of C<sub>60</sub> (**2a**)

In a 10 mL capped vial under a nitrogen inert atmosphere, a solution of [Rh(cod)<sub>2</sub>]BF<sub>4</sub> (2.8 mg, 0.0069 mmol) and (*R*)-Tol-BINAP (4.9 mg, 0.0072 mmol) in anhydrous CH<sub>2</sub>Cl<sub>2</sub> (4 mL) was prepared. Hydrogen gas was bubbled into the catalyst solution for 30 min before it was concentrated to dryness, dissolved in anhydrous *o*-DCB, and transferred via syringe into a solution of C<sub>60</sub> (50.5 mg, 0.07 mmol, 1 equiv.) and 1,6-enyne **1a** (72.2 mg, 0.21 mmol, 3 equiv.) in anhydrous *o*-DCB (1.4 mM), preheated to 90 °C. The resulting mixture was stirred at 90 °C for 30 min (TLC monitoring). The reaction mixture was purified by column chromatography using CS<sub>2</sub> as the eluent to provide unreacted C<sub>60</sub> (16.7 mg). Further elution with hexanes/EtOAc (9:1) followed by hexanes/toluene (1:1) gave compound **2a** as a dark brown solid (41.3 mg, 56% yield; 83% yield based on consumed C<sub>60</sub>).

### Experimental Procedure for the Synthesis of Hydroperoxide Derivative **3g**

In a 50 mL round bottom flask with a magnetic stirrer, a solution of **2g** (26.3 mg, 0.027 mmol) in toluene (15 mL) was

exposed to light and air for 7 h. The resulting solution was purified by column chromatography on silica gel using mixtures of toluene/dichloromethane (10:0 to 0:10) as the eluent to afford **3g** (7.8 mg, 29%) as a brown solid.

### Experimental Procedure for the Reduction of **3g** to **4g**

In a 50 mL round bottom flask with a magnetic stirrer, a solution of **3g** (21.9 mg, 0.022 mmol), PPh<sub>3</sub> (17.9 mg, 0.068 mmol) and toluene (15 mL) was stirred for 3 h at room temperature. The resulting solution was purified by column chromatography on silica gel using mixtures of toluene/dichloromethane (10:0 to 0:10) as the eluent to afford **4g** (20.7 mg, 96%) as a brown solid.

### Computational Details

Geometries of all stationary points were optimized without symmetry constraint with the Gaussian 16 program<sup>[24]</sup> using the DFT B3LYP hybrid exchange-correlation functional<sup>[25]</sup> employing the all-electron cc-pVDZ basis set.<sup>[26]</sup> The D3 Grimme energy corrections for dispersion<sup>[27]</sup> with the original damping function were added. The electronic energy was improved by performing single point energy calculations with the cc-pVTZ basis set<sup>[28]</sup> and the same density functional. Analytical Hessians were computed to determine the nature of stationary points (one and zero imaginary frequencies for TSs and minima, respectively) and to calculate unscaled zero-point energies (ZPEs) as well as thermal corrections and entropy effects using the standard statistical-mechanics relationships for an ideal gas.<sup>[29]</sup> These two latter terms were computed at 363.15 K and 1 atm to provide the reported relative Gibbs energies. Solvent effects were computed with the solvent model based on density (SMD) continuum solvation.<sup>[30]</sup> As a summary, the reported Gibbs energies contain electronic energies including solvent effects calculated at the B3LYP-D3/cc-pVTZ(SMD=o-DCB)//B3LYP-D3/cc-pVDZ level together with gas phase thermal and entropic contributions computed at 363.15 K and 1 atm with the B3LYP-D3/cc-pVDZ method.

### Supporting Information

Experimental procedures, compound characterization data including NMR spectra for all compounds. Xyz Cartesian coordinates, energies, and vibrational frequencies of all optimized complexes can be accessed via the ioChem-BD repository.<sup>[31]</sup> (See Supporting Information).

### Acknowledgements

We are grateful for the financial support from the Ministerio de Ciencia e Innovación and the EU (Project PID2020-113711GB-I00 MCIN/AEI/10.13039/50110001103, FPI predoctoral grant to C.C. and Margarita Salas grant (NextGenerationEU) to A.A.) and the Generalitat de Catalunya (Project 2021-SGR-623). Open Access funding provided thanks to the CRUE-CSIC agreement with Wiley.

### References

- [1] a) E. Castro, A. H. Garcia, G. Zavala, L. Echegoyen, *J. Mater. Chem. B* **2017**, *5*, 6523–6535; b) F. Cataldo, T. Da Ros, in: *Medicinal Chemistry and Pharmacological Potential of Fullerenes and Carbon Nanotubes* (Eds.: F. Cataldo, T. Da Ros), Springer Netherlands: Dordrecht, **2008**; Vol. 1; c) N. Panwar, A. M. Soehartono, K. K. Chan, S. Zeng, G. Xu, J. Qu, P. Coquet, K. T. Yong, X. Chen, *Chem. Rev.* **2019**, *119*, 9559–9656; d) J. Ramos-Soriano, J. J. Reina, B. M. Illescas, N. de la Cruz, L. Rodríguez-Pérez, F. Lasala, J. Rojo, R. Delgado, N. Martín, *J. Am. Chem. Soc.* **2019**, *141*, 15403–15412.
- [2] a) A. Montellano López, A. Mateo-Alonso, M. Prato, *J. Mater. Chem.* **2011**, *21*, 1305–1318; b) D. Canevet, E. M. Pérez, N. Martín, *Angew. Chem. Int. Ed.* **2011**, *50*, 9248–9259.
- [3] a) S. Collavini, J. L. Delgado, *Sustain. Energy Fuels* **2018**, *2*, 2480–2493; b) L. Jia, M. Chen, S. Yang, *Mater. Chem. Front.* **2020**, *4*, 2256–2282; c) O. Fernandez-Delgado, P. S. Chandrasekhar, N. Cano-Sampaio, Z. C. Simon, A. R. Puente-Santiago, F. Liu, E. Castro, L. Echegoyen, *J. Mater. Chem. C* **2021**, *9*, 10759–10767; d) M. Izquierdo, B. Platzer, A. J. Stasyuk, O. A. Stasyuk, A. A. Voityuk, S. Cuesta, M. Solà, D. M. Guldi, N. Martín, *Angew. Chem. Int. Ed.* **2019**, *58*, 6932–6937.
- [4] a) W. Śliwa, *Fullerene Sci. Technol.* **1995**, *3*, 243–281; b) I. Fernández, M. Solà, F. M. Bickelhaupt, *Chem. Eur. J.* **2013**, *19*, 7416–7422.
- [5] R. Taylor, *C. R. Chim.* **2006**, *9*, 982–1000.
- [6] a) A. Hirsch, I. Lamparth, T. Grosser, *J. Am. Chem. Soc.* **1994**, *116*, 9385–9386; b) R. Schwenninger, T. Muller, B. Krautler, *J. Am. Chem. Soc.* **1997**, *119*, 9317–9318; c) G. Pareras, S. Simon, A. Poater, M. Solà, *J. Org. Chem.* **2022**, *87*, 5149–5157.
- [7] Selected references: a) A. R. Tuktarov, A. R. Akhmetov, L. M. Khalilov, U. M. Dzhemilev, *Rus. Chem. Bull., Int. Ed.* **2010**, *59*, 611–614; b) Q. Liu, T.-X. Liu, J. Ma, G. Zhang, *Org. Lett.* **2020**, *22*, 284–289; c) J. Ma, T.-X. Liu, P. Zhang, C. Zhang, G. Zhang, *Chem. Commun.* **2021**, *57*, 49–52; d) T.-X. Liu, X. Wang, P. Zhang, P. Yang, X. Li, G. Zhang, *Org. Lett.* **2022**, *24*, 9102–9106.
- [8] a) A. Artigas, A. Pla-Quintana, A. Lledó, A. Roglans, M. Solà, *Chem. Eur. J.* **2018**, *24*, 10653–10661; b) E. Castro, A. Artigas, A. Pla-Quintana, A. Roglans, F. Liu, F. Perez, A. Lledó, X.-Y. Zhu, L. Echegoyen, *Materials* **2019**, *12*, 1314.
- [9] A. Artigas, C. Castanyer, N. Roig, A. Lledó, M. Solà, A. Pla-Quintana, A. Roglans, *Adv. Synth. Catal.* **2021**, *363*, 3835–3844.
- [10] a) B. M. Trost, M. Lautens, *J. Am. Chem. Soc.* **1985**, *107*, 1781–1783; b) B. M. Trost, *Acc. Chem. Res.* **1990**, *23*, 34–42.
- [11] Selected reviews: a) B. M. Trost, M. J. Krische, *Synlett* **1998**, 1–16; b) C. Aubert, O. Buisine, M. Malacria, *Chem. Rev.* **2002**, *102*, 813–834; c) G. C. Lloyd-Jones, *Org. Biomol. Chem.* **2003**, *1*, 215–236; d) S. T. Diver, A. J. Giessert, *Chem. Rev.* **2004**, *104*, 1317–1382; e) L.

- Zhang, J. Sun, S. A. Kozmin, *Adv. Synth. Catal.* **2006**, *348*, 2271–2296; f) V. Michelet, P. Y. Toullec, J.-P. Genêt, *Angew. Chem. Int. Ed.* **2008**, *47*, 4268–4315; g) E. Jiménez-Núñez, A. M. Echavarren, *Chem. Rev.* **2008**, *108*, 3326–3350; h) A. Marinetti, H. Jullien, A. Voituriez, *Chem. Soc. Rev.* **2012**, *41*, 4884–4908; i) I. D. G. Watson, F. D. Toste, *Chem. Sci.* **2012**, *3*, 2899–2919; j) C. I. Stathakis, P. L. Gkizis, A. L. Zografos, *Nat. Prod. Rep.* **2016**, *33*, 1093–1117; k) Y. Hu, M. Bai, Y. Yang, Q. Zhou, *Org. Chem. Front.* **2017**, *4*, 2256–2275; l) A. M. Echavarren, C. Nevado, *Chem. Soc. Rev.* **2004**, *33*, 431–436.
- [12] Selected reviews: a) T. Shibata, *Adv. Synth. Catal.* **2006**, *348*, 2328–2336; b) H.-W. Lee, F.-Y. Kwong, *Eur. J. Org. Chem.* **2010**, 789–811; c) A. Lledó, X. Verdager, A. Riera, in: *The Pauson-Khand Reaction: Scope, Variations and Applications* (Ed. R. R. Torres), Wiley, Hoboken, **2012**, pp. 147–180; d) S. Chen, C. Jiang, N. Zheng, Z. Yang, L. Shi, *Catalysis* **2020**, *10*, 1199; e) Z. Yang, *Acc. Chem. Res.* **2021**, *54*, 556–568.
- [13] Selected examples: a) T. Shibata, Y. Arai, Y.-K. Tahara, *Org. Lett.* **2005**, *7*, 4955–4957; b) T. N. Tekavec, J. Louie, *J. Org. Chem.* **2008**, *73*, 2641–2648; c) P. A. Evans, J. R. Sawyer, P. A. Inglesby, *Angew. Chem. Int. Ed.* **2010**, *49*, 5746–5749; d) R. Liu, L. Giordano, A. Tenaglia, *Chem. Asian J.* **2017**, *12*, 2245–2257; e) J. Ni, J. Chen, Y. Zhou, G. Wang, S. Li, Z. He, W. Sun, B. Fan, *Adv. Synth. Catal.* **2019**, *361*, 3543–3547; f) Q. Teng, W. Mao, D. Chen, Z. Wang, C.-H. Tung, Z. Xu, *Angew. Chem. Int. Ed.* **2020**, *59*, 2220–2224; g) S. Suzuki, Y. Shibata, K. Tanaka, *Chem. Eur. J.* **2020**, *26*, 3698–3702; h) T. Yasui, Y. Nakazato, K. Kurisaki, Y. Yamamoto, *Adv. Synth. Catal.* **2021**, *363*, 4182–4189.
- [14] Selected examples: a) H. Zheng, Y. Wang, C. Xu, Q. Xiong, L. Lin, X. Feng, *Angew. Chem. Int. Ed.* **2019**, *58*, 5327–5331; b) Y. Yamamoto, H. Hayashi, T. Saigoku, H. Nishiyama, *J. Am. Chem. Soc.* **2005**, *127*, 10804–10805; c) D. Bentz, S. Laschat, *Synthesis* **2000**, 1766–1773.
- [15] N. Martín, M. Altable, S. Filippone, A. Martín-Domech, M. Güell, M. Solà, *Angew. Chem. Int. Ed.* **2006**, *45*, 1439–1442.
- [16] M. Ishida, Y. Shibata, K. Noguchi, K. Tanaka, *Chem. Eur. J.* **2011**, *17*, 12578–12581.
- [17] M. Ishida, K. Tanaka, *Org. Lett.* **2013**, *15*, 2120–2123.
- [18] a) M. Stratakis, M. Orfanopoulos, *Tetrahedron* **2000**, *56*, 1595–1615; b) D. A. Singleton, C. Hang, M. J. Szymanski, M. P. Meyer, A. G. Leach, K. T. Kuwata, J. S. Chen, A. Greer, C. S. Foote, K. N. Houk, *J. Am. Chem. Soc.* **2003**, *125*, 1319–1328; c) M. Prein, W. Adam, *Angew. Chem. Int. Ed.* **1996**, *35*, 477–494.
- [19] a) Y.-Z. An, G. A. Ellis, A. L. Viado, Y. Rubin, *J. Org. Chem.* **1995**, *60*, 6353–6361; b) Y.-Z. An, A. L. Viado, M. J. Arce, Y. Rubin, *J. Org. Chem.* **1995**, *60*, 8330–8331; c) N. Chronakis, G. Froudakis, M. Orfanopoulos, *J. Org. Chem.* **2002**, *67*, 3284–3289; d) N. Chronakis, G. C. Vougioukalakis, M. Orfanopoulos, *Org. Lett.* **2002**, *4*, 945–948.
- [20] a) S. Kozuch, S. Shaik, *J. Am. Chem. Soc.* **2006**, *128*, 3355–3365; b) S. Kozuch, S. Shaik, *Acc. Chem. Res.* **2011**, *44*, 101–110.
- [21] N. E. Schore, *Chem. Rev.* **1988**, *88*, 1081–1119.
- [22] A. Artigas, J. Vila, A. Lledó, M. Solà, A. Pla-Quintana, A. Roglans, *Org. Lett.* **2019**, *21*, 6608–6613.
- [23] Reactions involving **1a** or **1g** and rhodium catalyst without C<sub>60</sub> resulted in the formation of a complex mixture of cycloisomerized derivatives from which diene **I** was not detected.
- [24] Gaussian 16, Revision C.01, M. J. Frisch, G. W. Trucks, H. B. Schlegel, G. E. Scuseria, M. A. Robb, J. R. Cheeseman, G. Scalmani, V. Barone, G. A. Petersson, H. Nakatsuji, X. Li, M. Caricato, A. V. Marenich, J. Bloino, B. G. Janesko, R. Gomperts, B. Mennucci, H. P. Hratchian, J. V. Ortiz, A. F. Izmaylov, J. L. Sonnenberg, D. Williams-Young, F. Ding, F. Lipparini, F. Egidi, J. Goings, B. Peng, A. Petrone, T. Henderson, D. Ranasinghe, V. G. Zakrzewski, J. Gao, N. Rega, G. Zheng, W. Liang, M. Hada, M. Ehara, K. Toyota, R. Fukuda, J. Hasegawa, M. Ishida, T. Nakajima, Y. Honda, O. Kitao, H. Nakai, T. Vreven, K. Throssell, Montgomery, J. A., Jr., J. E. Peralta, F. Ogliaro, M. J. Bearpark, J. J. Heyd, E. N. Brothers, K. N. Kudin, V. N. Staroverov, T. A. Keith, R. Kobayashi, J. Normand, K. Raghavachari, A. P. Rendell, J. C. Burant, S. S. Iyengar, J. Tomasi, M. Cossi, J. M. Millam, M. Klene, C. Adamo, R. Cammi, J. W. Ochterski, R. L. Martin, K. Morokuma, O. Farkas, J. B. Foresman, D. J. Fox, Gaussian, Inc., Wallingford CT, 2016.
- [25] a) P. J. Stephens, F. J. Devlin, C. F. Chabalowski, M. J. Frisch, *J. Phys. Chem.* **1994**, *98*, 11623–11627; b) A. D. Becke, *J. Chem. Phys.* **1993**, *98*, 5648–5652; c) C. Lee, W. Yang, R. G. Parr, *Phys. Rev. B* **1988**, *37*, 785–789.
- [26] T. H. Dunning, *J. Chem. Phys.* **1989**, *90*, 1007–1023.
- [27] S. Grimme, J. Antony, S. Ehrlich, H. A. Krieg, *J. Chem. Phys.* **2010**, *132*, 154104.
- [28] R. A. Kendall, T. H. Dunning Jr, R. J. Harrison, *J. Chem. Phys.* **1992**, *96*, 6796–6806.
- [29] P. Atkins, J. De Paula, *The Elements of Physical Chemistry*, 3rd ed.; Oxford University Press: Oxford, **2006**.
- [30] A. V. Marenich, C. J. Cramer, D. G. Truhlar, *J. Phys. Chem. B* **2009**, *113*, 6378–6396.
- [31] M. Álvarez-Moreno, C. de Graaf, N. López, F. Maseras, J. M. Poblet, C. Bo, *J. Chem. Inf. Model.* **2015**, *55*, 95–103.